UNIVERSITÀ DEGLI STUDI DI PALERMO
Dottorato di ricerca in Oncologia e Chirurgia Sperimentali
Dipartimento di Discipline Chirurgiche Oncologiche e Stomatologiche (Di.Chir.On.S.)

Polybutylene succinate scaffold for bone tissue: in vivo study in rabbit

Doctoral Dissertation of:
Dr. Giulio Edoardo Vigni

Tutor:
Prof.ssa Olga Di Fede

Co-Tutor:
Prof. Lawrence Camarda

The Chair of the Doctoral Program:
Prof. Antonio Russo

Cycle XXXVII

INDEX

CHAPTER 1

Introduction: Background Rationale and Objectives

In recent years, tissue engineering has become the focus of regenerative medicine through the study and research of biomaterials capable of stimulating tissue growth, mimicking its characteristics, and accelerating healing.

Bone defects represent one of the greatest challenges in this field and, especially in recent years, tissue engineering is an area of great interest in its application to orthopaedic surgery.

Despite its high healing potential, spontaneous healing of major bone defects, such as those following tumor resection, infection, or severe trauma, is almost never possible. Although allogeneic and xenogeneic grafts are used for these purposes, the gold standard is autogenous transplantation, especially from the iliac bones [1]. Although this technique is widely used, it has several critical issues: the conformity of the graft shape to the defect, the increase in surgical time, the resorption of the graft, the insufficient or non-availability of tissue, as in children, and comorbidities related to the graft harvest site.

This creates the motivation for the development of substitute materials, the scaffolds. These are engineered tissues, manufactured using suitable biocompatible materials and containing stem or tissue-specific cells, and have the ability to mimic and support bone biological functions.

Tissue engineering finds three-dimensional scaffolds to be one of the most promising resources for bone tissue regeneration. These biomaterials must have specific characteristics, such as high mechanical strength or physical properties suited to the form and function of the bone structure into which they are to be implanted [2]. In 2018, Preethi Soundarya S et al [3] provided an overview of the different fabrication techniques for the preparation of scaffolds (biological macromolecules such as chitin/ chitosan, collagen/gelatin, alginate, hyaluronic acid, silk, synthetic polymers, ceramics). The study, analysing more than 40 different techniques and compositions, showed good results but concluded that an ideal production method for a scaffold has yet to be defined.

Besides creation, the actual in vivo applicability of any scaffold relies on confirmation of the biocompatibility and biodegradability of the material used. An excessive inflammatory response can impair tissue healing capacity and degradation derivatives can provoke immunogenic reactions. Therefore, as highlighted by a study published in 2019 [4], understanding the degradation characteristics of various biomaterials and non-invasive monitoring of implanted scaffolds is necessary.

Not least, scaffold-based tissue engineering must also take into account both pore size and mechanical properties: an increase in pore size is generally accompanied by a decrease in mechanical strength [2]. In order to achieve adequate mechanical properties and porosity, Derja Algul et al.'s 2015 study [5] investigated the possibility of using a biomimetic

monolithic three-layer scaffold with chitosan, alginate, and β-TCP, mimicking the structure of spongy bone and cortical bone. Characterisation results showed the existence of strong ionic interactions between the layers, indicating that these scaffolds were considered non-toxic and therefore suitable for osteochondral implants.

A 2019 Korean study compared two structural models of 3D-printed scaffolds. On a calvarial bone defect model in the rabbit, a scaffold with a conventional grid structure and one with a kagome-like structure were compared. The research showed that the kagome structure provided excellent mechanical robustness and better osteoconductivity than the control group, thus laying the foundation for future studies on the geometry of the basic scaffold structure as well [6].

However, not all potentially biocompatible materials have proven to be applicable. For example, Lim et al. demonstrated that the implantation of their scaffold prevented bone regeneration, even in a non-critical bone defect [7]. In contrast, others such as Maeda et al. studied a material already widely used in human surgery, hydroxyapatite, to make biocompatible scaffolds [8].

To date, the ideal scaffold has not yet been realised [3], so scientific research also focuses on engineering the available ones. The aim is to enhance the effect of scaffolds and at the same time counteract the specific limitations of certain materials.

For example, Ma et al. studied a scaffold on the tibia in vivo in rabbits, trying to counteract the lack of angiogenic properties and undesirable mechanical properties, such as brittleness, of hydroxyapatite. They created a polyvinyl-alcohol/collagen/nanoattapulgite/hydroxyapatite composite scaffold, and, with the synergistic effects of these elements, they demonstrated the promotion of vascularisation and bone formation [9].

In 2024, on the basis of the same assumptions, and again with the aim of inducing angiogenesis, Li et al. studied a new 3D-printed scaffold based on hydroxyapatite/carboxymethyl chitosan/polydopamine/total flavonoids from Rhizoma Drynariae [10]. In 2023, Ray et al. used scaffolds composed of *Antheraea mylitta* silk fibroin and chitosan on tibia defects [11].

In 2018, a Chinese research group [12], on a rabbit animal model with radial defect, demonstrated that an enhanced osteogenic effect could be achieved by using an engineered scaffold with mimetic osteoinductive periosteum. In 2017, a review by Hwan D Kim [13] showed that incorporating osteoinductive and osteoconductive materials, such as calcium and phosphate, into 3D scaffolds stimulates osteogenic differentiation of stem cells. Furthermore, it was shown that increasing the local concentration of phosphate ions in the scaffolds promoted the activation of transcription factors, such as osteocalcin and osteopontin, which induce osteogenic differentiation in stem cells. The same result was obtained using biodegradable polymeric scaffolds composed of calcium

phosphate and bone formation-related growth factors (BMP-2 and TGF-β3).

Bone substitutes with antibiotics, on the other hand, find specific application in orthopaedic and trauma surgery for the prevention or treatment of bone infections. However, their use as bone grafts revealed some concerns due to their rapid biodegradation [14]. The addition of calcium carbonate and tripalmitin made calcium sulphate formulations more resistant to resorption. Pförringer et al. [14] in 2018 implanted calcium sulphate and antibiotic scaffolds into the tibial metaphysis of rabbits, demonstrating excellent biocompatibility and the ability to improve mechanical stability.

In 2020, Teotia et al. [15] compared in vivo the use of 3D-printed porous composite scaffolds with resins and osteoinductive growth factors in critical bone defects on flat (cranial theca) and long bones (tibia) in rabbits. The tibia study involved fewer samples than the cranium study, but compared to the control group without scaffolds, faster healing of bone defects in both types of bones was demonstrated. Kalay et al. in 2022 studied bone defects of the tibia with distraction osteogenesis [16]. After tibial osteotomy, they placed an external fixator, increasing the distraction by 0.6 mm every day for 26 days. Control and engineered groups with BMP-2 and deferoxamine (DFO) were compared. The increase in VEGF activity, given by the growth factors, efficiently stimulated angiogenesis but without showing significant differences with the control group. Even though the

BMP-2 group proved to have the highest load-to-failure, the results showed that the mechanical stability of the external fixator was the fundamental condition for bone healing. Hence, growth factors in a biomechanically unfavourable condition may not be sufficient for favourable bone regeneration. This study confirmed that the mechanical support of the scaffold element is crucial.

Numerous studies aim to enhance the osteoinductive and osteoconductive activity of scaffolds. Of all the molecules proposed, one of the most widely used growth factors is BMP-2, Bone Morphogenetic Protein-2. This is a growth factor known for its osteoinductive properties and is shown to promote the differentiation of stem cells into bone tissue. In vitro studies show that BMP-2 increases angiogenesis in fracture healing by stimulating the expression of differentiation markers (osteocalcin, alkaline phosphatase), mineralised bone nodules [17,18], and VEGF secretion in osteoblasts [19,20].

However, BMP-2 has a very short half-life, usually between 7 and 16 minutes, making the application of high doses necessary to achieve clinical efficacy [21]. The use of supraphysiological doses of BMP-2 is associated with adverse effects, including heterotopic bone formation and inflammation [22]. To minimise these side effects, carriers capable of continuously releasing an adequate amount of BMP-2 are needed. In clinical practice, bioceramics such as hydroxyapatite and beta-TCP, as well

as materials like collagen membranes, are used as vectors for the release of BMP-2 [23-25].

Han et al., in 2021, investigated a novel 3D-printed polylactic acid (PLA) porous scaffold and a combination of recombinant human bone morphogenetic protein-2 (rhBMP-2) and/or mesenchymal stem cells (MSCs) with a biogel composed of gelatin and alginate [26]. Go's group in 2018 also proved the efficacy of BMP-2 by genetically manipulating teratoma-derived fibroblast (TDF) cells with the simultaneous introduction of BMP-2 and genes coding for herpes simplex virus thymidine kinase (HSV-tk) [27]. The already high self-production of BMP-2 in TDF cells strongly increased alkaline phosphatase (ALP) activity, calcium content, and mRNA expression of osteogenic marker genes during osteogenesis in vitro. The clinical efficacy of this strategy was then proven with significantly increased bone formation volume in rabbit models of calvarial and femoral bone defects of critical size.

Yoon et al. demonstrated the efficacy of BMP-2 protein in non-structural scaffolds [28]. They created injectable hydrogels based on visible light-polymerised glycol chitosan (GC) hydrogels containing BMP-2 and/or transforming growth factor-beta1 (TGF-β1). Their application on rat tibia confirmed the ability of this molecule to increase bone formation.

The effects of scaffolds incorporating BMP-2 are extensively studied in preclinical and clinical studies, especially on collagen-based scaffolds. However, there is still room for improving therapeutic results and finding

the most suitable scaffold combination [29-31]. Regarding BMP-2 efficacy, Kalay showed that, compared to DFO and a control group, healing a bone defect with BMP-2 had a higher load-to-failure in the ‘3-point bending test’ [32]. At the same time, it was emphasised that mechanical stability is the fundamental condition for bone healing.

The recent literature emphasises the need to find a biocompatible scaffold with the appropriate mechanical capacity that can be used as a substrate for integrating growth factors such as BMP-2.

These considerations cannot be separated from optimising the ‘product’ for its end use. The ideal scaffold must go through further steps, starting with its applicability in the surgical field, specifically orthopaedics. Subsequent steps include production and cost optimisation for large-scale distribution.

In 2021, the author, in a project with Cicero et al. [33], studied a 3D micro-fibrillar scaffold based on PBS (poly 1,4-butylene succinate) produced by electrospinning, without the addition of growth factors, in sciatic nerve lesions on a mouse model. The study confirmed the biocompatibility and biodegradability of the scaffold. Furthermore, an improvement in peripheral nerve regenerative processes was demonstrated. These properties, combined with the ability to limit the action of macrophages and reduce inflammation, encouraged potential applications of this scaffold in other tissues.

To date, no PBS scaffold has been studied for bone defects.

This project proposes to investigate the potential applications of the 3D micro-fibrillar PBS-based scaffold to in vivo bone tissue in rabbits. The study compares bone regeneration between a study group treated with the proposed scaffold and a control group left to spontaneously heal after creating identical bone defects. The main objective is to evaluate the surgical applicability of the device and demonstrate its biocompatibility and biodegradability in bone tissue in vivo. A secondary objective is to evaluate the scaffold's osseointegration and its ability to improve bone regeneration.

A second part of the study aims to create an engineered scaffold with the BMP-2 protein to enhance its osteogenic activity, evaluating its new osteoinductive and osteoconductive capabilities. Implanting the scaffold on the tibia, the study also aims to evaluate its applicability, behaviour and mechanical response in a long bone, which differs in composition and loading stress from a flat bone such as the cranial theca.

CHAPTER 2

Materials and Methods

Part One: Cranial Theca

Scaffold preparation and characterization

PBS and its copolymers are semi-crystalline thermoplastic polymers belonging to the aliphatic polyester family [34]. Characteristics and properties of PBS are high crystallisation rates, wide application range between -30°C and 120°C, high flexibility, strength and insulating capacity [35]. Our PBS scaffold is produced as a random fiber material by electrospinning. PBS (Poly(1,4-butylene succinate) extended with 1,6-diisocyanatohexane - Sigma-Aldrich, UK) solution (15% w/v in 1,1,1,3,3,3-hexafluoroisopropanol) is collected by a precision 10 mL syringe and placed in an NF 103 Electrospinning (MECC, Fukuoka, Japan). The flow (1.2ml/h) passes through a PTFE tube and then in a steel flat needle (22 gauge) with a 15.5 cm gap between the needle tip and the collector. One high-voltage generator is employed with a positive voltage (+12.5 kV) to charge the steel capillary containing the polymer solution while the stainless-steel collector plate is maintained at ground voltage. The humidity is maintained in a range between 23% and 27%.

The morphological characteristics of scaffolds is investigated with a scanning electron microscope (SEM) (Phenom PRO X SEM) operating at 5 kV. Each sample is deposited onto a carbon-coated steel stub, dried under vacuum (0.1 Torr), and sputter-coated with 15-nm thick gold (Sputter Coater LuxorAu, Luxor Tech, Nazareth BELGIUM) prior to microscopy examination. The fiber morphology and diameters is evaluated using the ImageJ (1.52Q Wayne Rasband National Institute of Health, Bethesda, MD, USA) software.

3D structure of the scaffold is analyzed with a μCT scanner (Skyscan 1272, Bruker Kontich, Belgium) at a source voltage of 40 kV, a current of 250 mA, a total rotation of 180° and a rotation step of 0.3°. No filter mode is chosen for the acquisitions. The image pixel size is 2.6 μm and the scan duration is about 3 hr for every sample. The scanning dataset obtained after the acquisition step consists of images in 16-bit tiff format (3238 x 4904 pixels). The 3D reconstructions is carried out using the software NRecon (version 1.6.10.2) starting from the acquired projection images. The obtained 2D-images has a color depth of 8 bit with 265 grey levels. The whole set of raw images is displayed in a 3D space by the software CTVox.

Study population

After exploring alternatives to animal model testing in bone scaffold research in the literature and taking into account the guidance given by the

European Union Reference Laboratory for alternatives to animal testing (EU Reference Laboratory for alternatives to animal testing, EURL-ECVAM) on alternative methods and acceptable approaches, the animal model (rabbit) is used. Procedures involving animals are carried out in accordance with the Italian Legislative Decree N° 26/2014 and the European Directive 2010/63/EU. The animals experiment project is successfully approved by the Italian Ministry of Health with the following authorization n° 66-2022/PR dated 02/28/2022 (prot 28875.38).

The animals are housed and tested at the Istituto Zooprofilattico Sperimentale della Sicilia 'A. Mirri' with ministerial authorisation: 14/2015-UT.

The number of animals used for this project is reduced to the minimum compatible for the verification of the scientific objectives, compatible with the standards published in the literature that allows statistical evaluation.

The present in vivo study is conducted on 9 male New Zealand white rabbits from the company Harlan Laboratories srl Zona Industriale Azzida, 57 33049 - San Pietro al Natisone (UD), with an average body weight of 4.85 kg (range: 3.5-6 kg). A sample size of 9 rabbits is required to obtain a 98% power and an average SFI at least 15 points better than the control group. A one-sided two sample t-test is calculated with a significance level (alpha) of 0.05. Animals are housed in polypropylene cage and kept in controlled temperature (22 ± 2°C), humidity (50–55%) and light (12 hr light/ dark cycle). Animals have access to food and water ad libitum. Rabbits are

randomly divided into 3 groups of three individuals each and allowed to acclimate for at least 2 days prior to experiments.

Follow-ups are performed at 4, 12 and 24 weeks.

Surgical procedure

The experimental procedure is conducted under general anaesthesia and with the administration of analgesics and antibiotic therapy, so that no pain, suffering or stress is induced in the animal.

Animals are induced to anaesthetic depth with inhaled isoflurane at 2% and then anaesthetised with intramuscular (i.m.) injection of Zoletil(r) (tiletamine/zolazepam; 10 mg/kg) and Domitor(r) (medetomidine hydrochloride; 0.5 mg/kg.

The surgical procedure is performed by the same surgeon, in a sterile field after shaving and disinfecting the skin with iodine solution.

A full-thickness incision is made along the midline of the skull exposing both frontal and parietal bones. Retracted the skin flap, an approximately 8mm full-thickness circular defect is created on one frontal bone using a high-precision surgical drill (hand drill) under constant saline irrigation. An equal defect is created on the contralateral frontal bone. The diameter of the defects is checked with a ruler under microscopic vision.

All procedures are performed avoiding injury to the dura mater and underlying brain tissue. Then, the 8 mm x 2.5 mm scaffold is placed in one

of the randomly chosen bone defects without exerting any pressure on the underlying tissue (Figure 1).

Figure 1: Scaffold implantation into frontal bone defect.

At the end of the procedure, each subject has two bone defects. One defect is treated by applying the scaffold while the other is left to heal spontaneously. No suturing of the periosteum is performed. The skin is sutured with 3-0 silk and disinfected with iodine solution (Betadine).

Intramuscular atipamezole (Antisedan) (300 µg/kg) is used to awaken all rabbits. Carprofen (5 mg/kg) and Enrofloxacin (5 mg/kg) are daily administered for 1 week to each rabbit. After the procedure, each animal is assigned with an identification number and housed one per cage. They are

monitored on a daily basis for infection, self-mutilation, and signs of distress.

Radiological examination: CT evaluations

CT images are acquired with a Simens SOMATOM Definition AS machine, 128 banks, rotation time 0.5 seconds, maximum mAs 250, effective 100-120 mAs, Kilovolt (KV)120, thickness 1.2 mm with 0.6 mm interval, pitch 0.6. The B20fsmooth filter and W450C40 window is used.

The bone reconstruction is done with 0.6 mm thickness with 0.3 mm interval, B60fsharp filter, "osteo" window W1500C450.

As in the 2018 study by Pihlman H. et al. [36], the area of the defect covered by mineralised bone tissue is assessed by CT evaluation.

Histological evaluation

After the CT examination, the subjects are euthanised with Tranax (1 ml) intracardiacally. After shaving, a median incision is made to expose the frontal bones. Using a high-precision surgical burr, the frontal bones are then harvested (Figure 2).

Figure 2: Sampling of the frontal bones.

Specimens fixed and preserved in 10% buffered formalin, are decalcified using Na EDTA (10% w/v, pH 7.2), prior to histological analysis. The decalcified frontal bone samples are cut transversely in two at the centre of the defect. All samples are embedded in paraffin and sectioned at a thickness of 5.0 µm for staining with haematoxylin and eosin (H&E).

The resulting preparations are dried overnight in an oven at 37°C. They are sparged with xylene for 20 min. After a series of passages in decreasing alcohol (100°, 95°, 75° and 50°), the slides are washed in distilled water and then stained with haematoxylin and eosin. This is followed by dehydration in ascending alcohols (50°, 75°, 95° and 100°) and

clarification in xylene. After this step, the slides are mounted in acrylic mounting medium (Eukitt®, O. Kindler GmbH).

The stained samples are analysed for tissue infiltration, bone formation patterns and scaffold integration. Images of the stained slides are obtained with a Leica DMR microscope equipped with a Leica DFC 320 digital camera and analysed using digital image analysis (Nikon NIS Br, Nikon Instruments Europe BV, Amsterdam, The Netherlands).

Immunohistochemical evaluation of the samples is also performed for CD56 to assess the presence of osteoblasts, CD68 to assess the presence of osteoclasts and CD34 to assess the presence of microvessels.

Statistical analysis

All experiments are performed in triplicate by collecting for each experiment a number of samples n = 3, and values are expressed as mean ± standard deviation. The collected data are analysed within each group and for the entire population using GraphPad PrismTM 4.0 software (GraphPad Software Inc., San Diego, CA, USA). The one-way ANOVA associated with Sidak's push-out test is used. All data are presented as mean and statistical significance is set at $p<0.05$.

Part Two: Tibia

Scaffold preparation and characterization

The PBS scaffold is produced following the procedure described in part one with some differences. PBS (Poly(1,4-butylene succinate) extended with 1,6-diisocyanatohexane, Sigma-Aldrich, UK) solution (15% w/v in 1,1,1,3,3,3-hexafluoroisopropanol) is mixed with hydroxyapatite powder (HA, 10% w/w respect to PBS weight, 75 mg) and the antibacterial molecule ciprofloxacine (CPX, 5% w/w respect to PBS, 37.5 mg) and used to prepare each batch of the scaffold. The electrospinning process is carried vertically with 15 kV voltage using a NF 103 Electrospinning (MECC, Fukuoka, Japan) and a constant polymeric solution rate (0.8 ml/ min) obtained through a programmable syringe pump. The electrospun scaffold is collected on a stainless-steel plate positioned 15 cm below the tip of the needle.

As in part one, the morphological characteristics of scaffolds are investigated with a scanning electron microscope (SEM) (Phenom PRO X SEM) and 3D structure of the scaffold is analyzed with a μCT scanner.

Loading of bone morphogenetic protein (BMP2)

Bone morphogenetic protein 2 (recombinant human BMP-2, 10 mcg, Merk) is loaded onto the scaffold using two different procedure: a printing deposition procedure and a droplet adsorption procedure.

The droplet adsorption procedure is a protein loading by impregnation. This is performed by depositing the protein solution, drop by drop, directly on the surface of the microporous scaffold and then dehydrating it under a sterile box for 24 hours.

To print bone morphogenetic protein 2 (recombinant human BMP-2, 10 mcg, Merk) an aqueous solution at the concentration of 5 mcg/mL, is created by using a precision printer, Dimatix DMP 2800 Fujifilm, equipped with piezoelectric nozzles capable of dispensing droplets of a few picoliters (approximately 5 pl). A single pulse waveform at 10 kHz jetting frequency is used for deposition, obtaining satellites-free spherical droplets with speeds higher than 5 m/s in the volume range of approximately few picoliters by setting a jetting voltage of 14 Volts.

The deposition of the BMP-2 protein ink on the scaffold is carried out by a series of layers in order to completely print the BMP-2 ink (2 mL) loaded in the cartridge. The print design of BMP-2 has an additional important feature. The concentration gradient of the protein runs from the outside to the inside of the scaffold to facilitate cell adhesion from the peripheral bone, as shown in Figure 3.

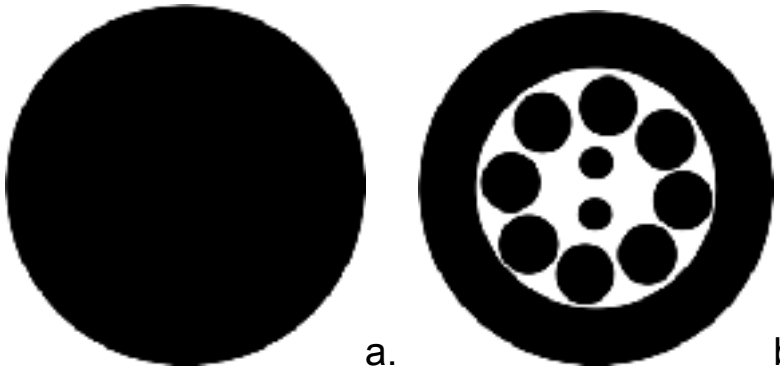

a. b.

Figure 3: printing patterns; pattern 1 (a) and pattern 2 (b).

To this end, the printing protocol is executed in two patterns. Pattern 1 (repeated for 30 layers, Figure 3a) evenly distributed the protein inks on the scaffold. Pattern 2 (repeated for 107 layers, Figure 3b) follows the pattern drawn in Figure 3b and produces the different concentration of protein on the scaffold. For both patterns, the distance between the drops is set at 5 microns in order to increase the density of the drops on the scaffold.

Study population

The regulatory and legislative references, as well as the authorisations, are the same as those applied for part one.

The number of animals used for this project is reduced to the minimum compatible with the verification of the scientific objectives, as required by the current legislation (Legislative Decree 26/2014).

This part of the study is conducted on 6 male New Zealand white rabbits from the company Harlan Laboratories srl Zona Industriale Azzida, 57 33049 - San Pietro al Natisone (UD), with an average body weight of 4.85 kg (range: 3.5-6 kg).

The rabbits are randomly divided into 3 groups of 2 individuals each and left to acclimatise for at least 2 days before the experiments. The groups are divided as follows. In the control group, the defect was left to heal spontaneously. Group A rabbits are those whose defect was treated with the printed protein scaffold. Lastly, Group B rabbits are those whose defect was treated with the impregnated protein scaffold.

Follow-ups are performed at 24 weeks.

Surgical procedure

The surgical procedure is performed under general anaesthesia following the same treatments and procedures described in part one, both pre- and post-operatively.

In a sterile field, after shaving and disinfecting the skin with iodine solution, a full-thickness incision is made along the frontal aspect of the proximal tibia. Retracting the skin flap and the periosteal sheet, an approximately 8mm circular defect is created on the frontal aspect of the cortical bone of the tibia using a high-precision surgical drill (hand drill).

Then a sterile spatula is used to create a cavity of approximately 5-6mm. After removing the correct amount of bone tissue, the defect is washed with saline solution.

All procedures are performed under constant saline irrigation to avoid friction damage to the bone. Then, the 8 mm scaffold is placed in the bone defect exerting a minimal pressure making the scaffold stable and covering the defect (Figure 4). No suturing of the periosteum is performed. The skin is sutured with 3-0 silk and disinfected with iodine solution (Betadine).

As in part one, after the procedure, each animal is assigned with an identification number and housed one per cage. They are monitored on a daily basis for infection, self-mutilation, and signs of distress.

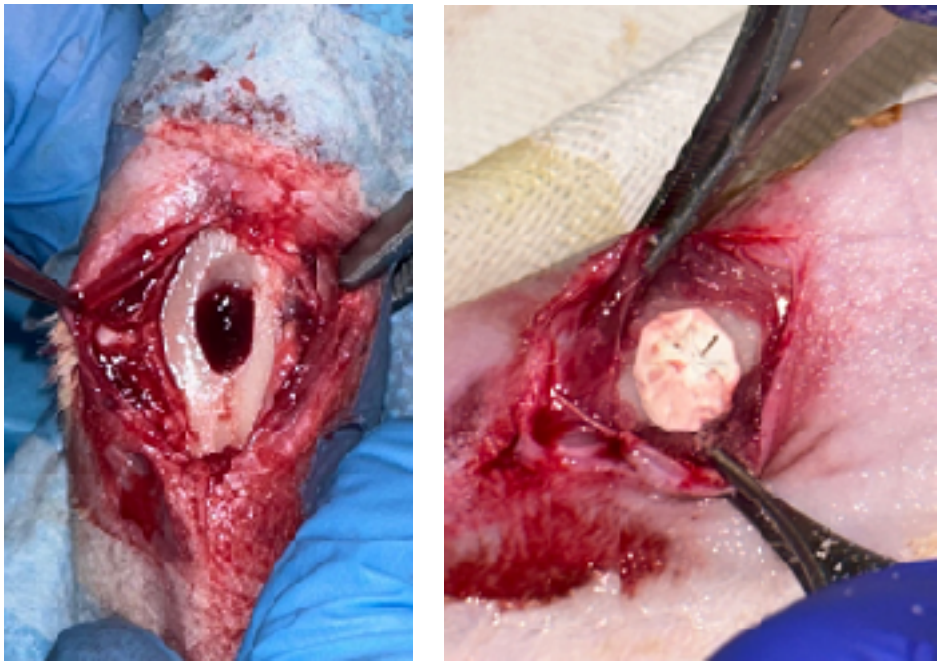

Figure 4: Application of the scaffold on the tibial defect.

Histological evaluation

At the follow-up, the subjects are euthanised with Tranax (1 ml) intracardiacally. After shaving, an incision on the anterior aspect of the tibia is made to expose the bone. Using a high-precision surgical burr, the bone is harvested (Figure 5).

Figure 5: Sampling of the tibia.

The histological examination is conducted using the same procedures and instruments as in the first part, with the exception of the following. The thickness of the sections is 4 μm. In addition, to measure the area of newly formed bone between the groups, three microscope images are obtained from three random areas of each sample.

Statistical analysis

A descriptive analysis was conducted to investigate the differences between the study groups and the control group.

s

CHAPTER 3

Results

Part One: Cranial Theca

Scaffold

Macroscopically, fiber deposition is smooth and homogeneous along the metal rod, without any gross defects (Figure 6). An almost linear relation between the thickness of the electrospun layer and the deposition time is observed. SEM is adopted as an investigation method to study the morphology and orientation of nanofibers. Observed under SEM (Figure 7,8), the scaffold appears as a random fiber mat characterized by fiber diameters in the range between 200nm and 1.5um. The scaffold has an average thickness of about 800 microns (measured on microCT, Figure 9) and sufficient rigidity for manipulation during implantation, as demonstrated in the photo (Figure 6). Therefore, it can be easily cut with scissors and adapted to the bone defect.

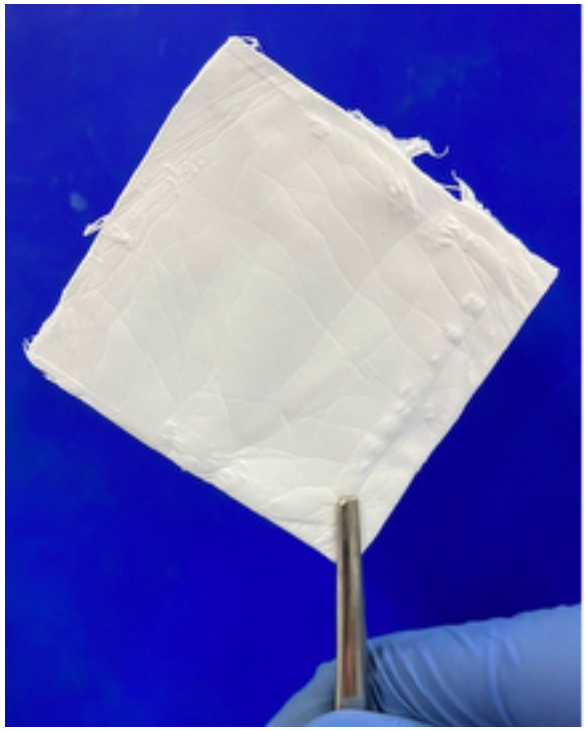

Figure 6: Photo of the scaffold.

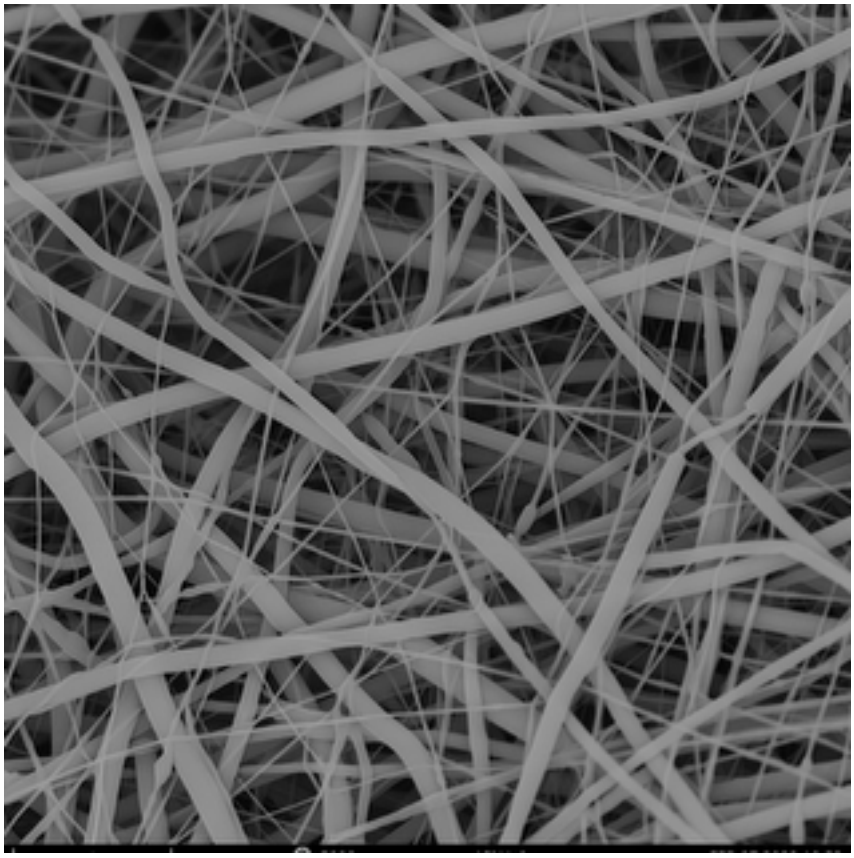

Figure 7: SEM image of electrospun PBS scaffold at 5000x magnification.

Figure 8: SEM image of electrospun PBS scaffold at 500x magnification.

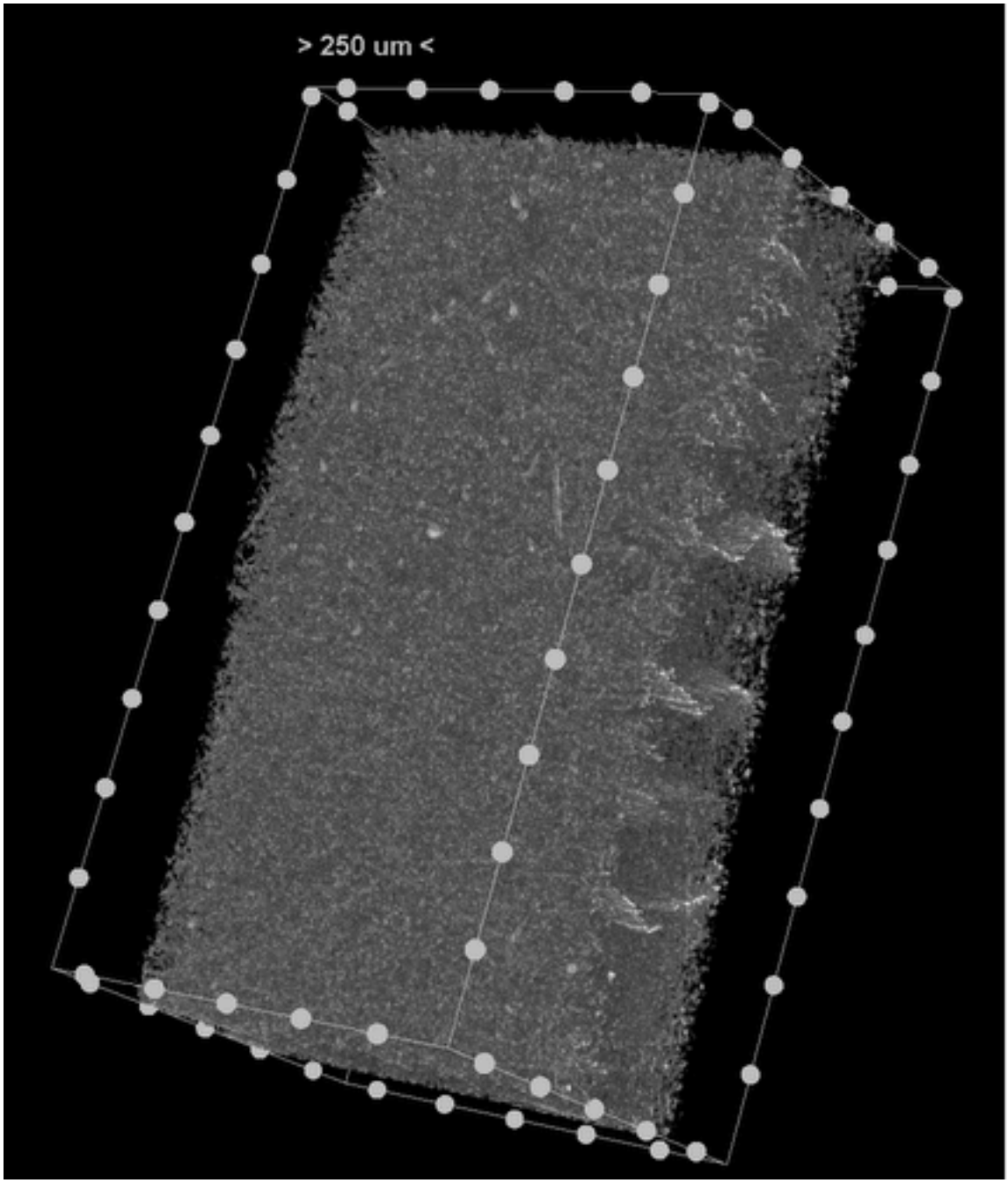

Figure 9: microCT reconstruction of PBS scaffold.

CT evaluation

Bone formation is assessed with CT scans at 4 (Figure 10), 12 (Figure 11), and 24 weeks (Figure 12).

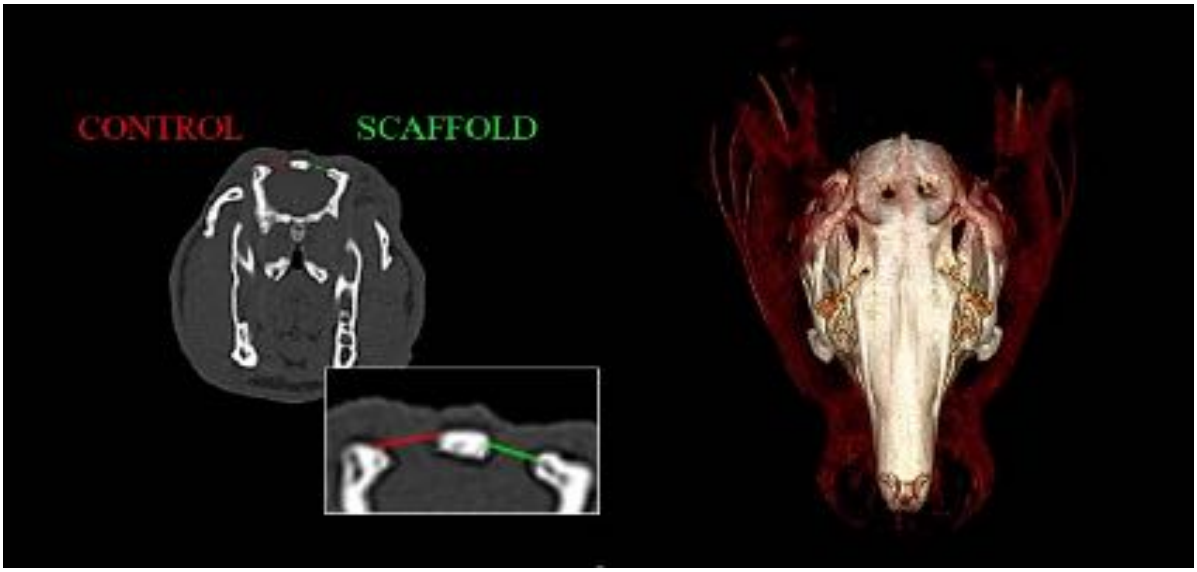

Figure 10: CT scan and 3D reconstruction at 4 weeks. A comparison of the diameters of treated versus untreated bone defects is demonstrated in the coronal view.

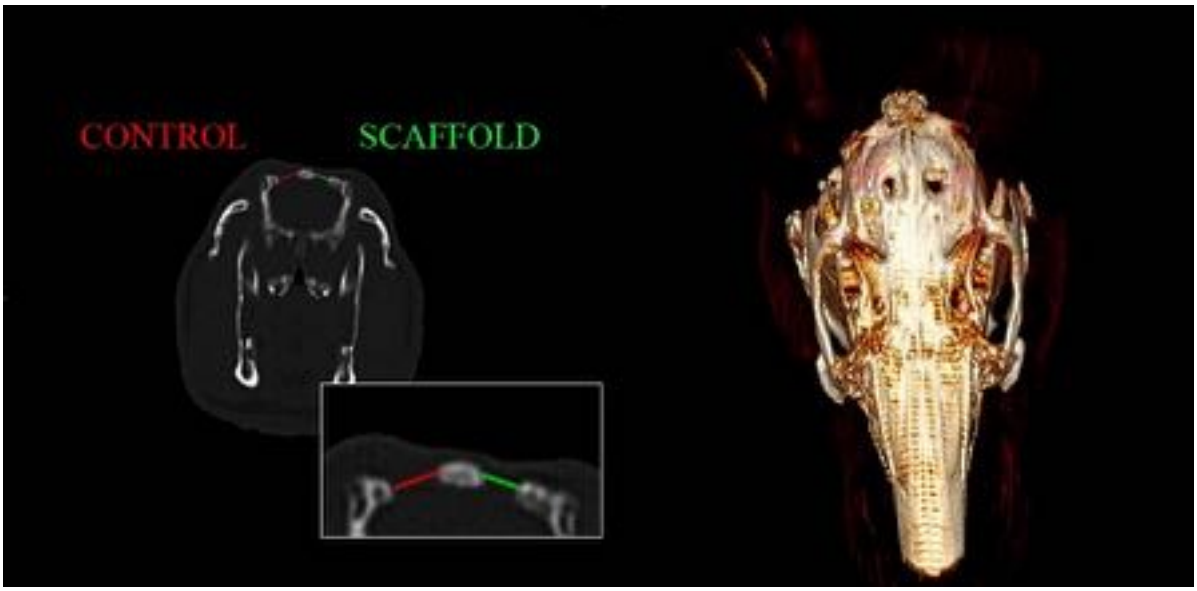

Figure 11: CT scan and 3D reconstruction at 12 weeks. A comparison of the diameters of treated versus untreated bone defects is demonstrated in the coronal view.

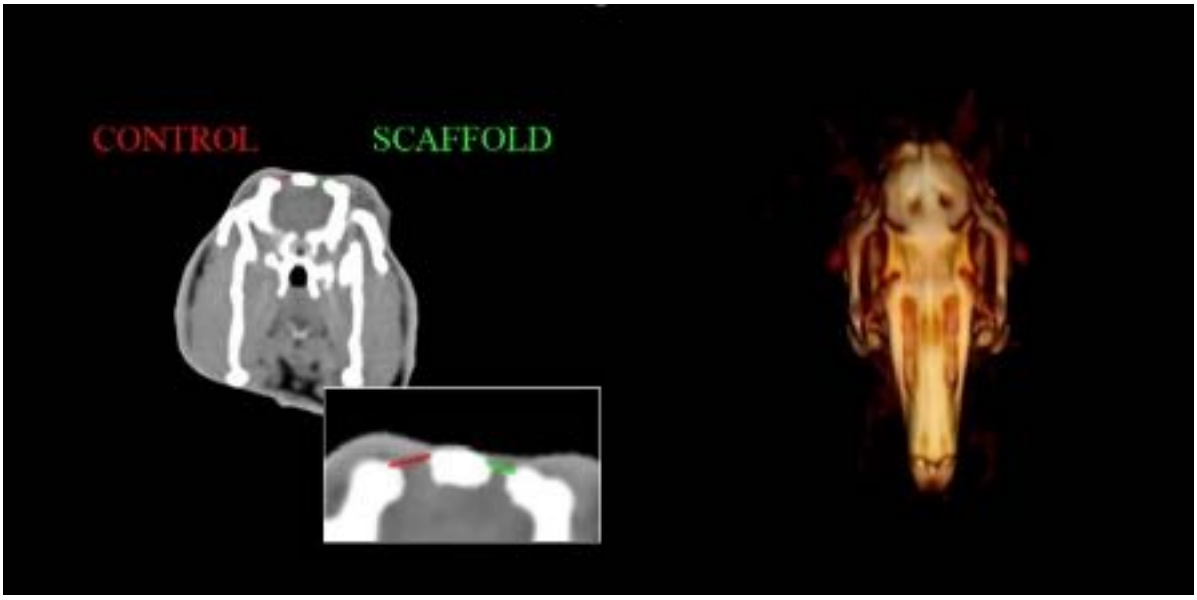

Figure 12: CT scan and 3D reconstruction at 24 weeks. A comparison of the diameters of treated versus untreated bone defects is demonstrated in the coronal view.

In the figures 10 to 12, 3D reconstructions and CT scans (in a similar position) of the bone defect are collected. There is a magnification of the scans with the defect measurement comparing the control side with the experimental side. The comparison in defect healing progression between the native process and scaffold application is shown in the following diagram (Figure 13).

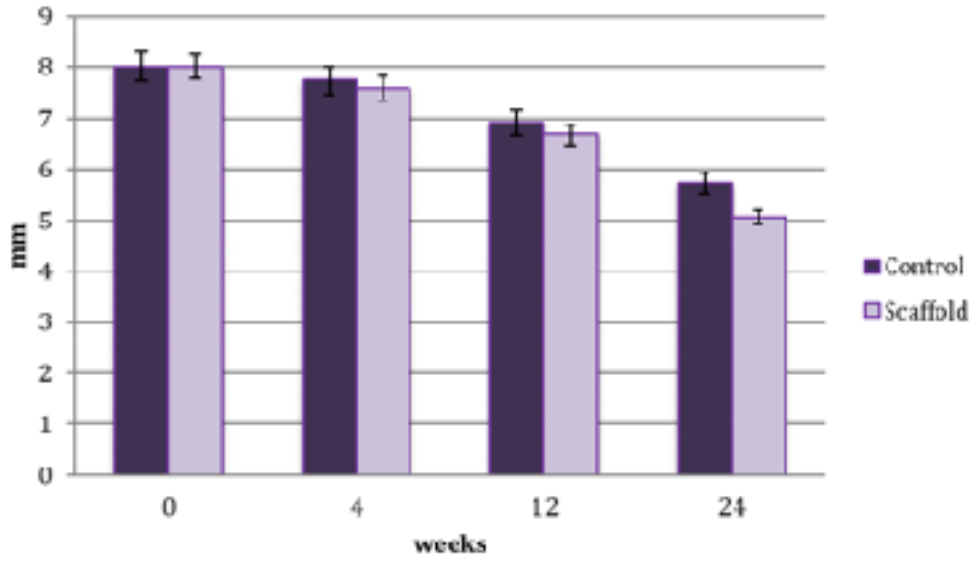

Figure 13. Comparison of the healing progression of the scaffold-treated and untreated (control) bone defect at 4, 12 and 24 weeks.

The statistical analysis, performed with Sidak's test on the values measured by CT scans, is described in Table 1.

Sidak's multiple comparisons test	Mean Diff	95,00% CI of diff.	Significant	Summary	Adjusted P Value
0w vs.4w	0,3400	-0,9136 to 1,594	no	ns	0,7218
0 w vs. 12 w	1,205	-0,0486 to 2,459	no	ns	0,0558
0 w vs. 24 w	2,605	1,351 to 3,859	yes	*	0,0061

4 w vs. 12 w	0,8650	-0,3886 to 2,119	no	ns	0,1336
4 w vs. 24 w	2,265	1,011 to 3,519	yes	*	0,0092
12 w vs. 24 w	1,400	0,1464 to 2,654	Yes	*	0,0367

Table 1: Statistical Analysis on bone defects' diameters measured using CT scans.

The bone regeneration that occurred from 4 to 24 weeks, from 12 to 24 weeks and in the total interval from 0 to 24 weeks is statistically significant (p value<0.05) in both the control and scaffold-treated defects. No statistically significant results, also due to a limited number of samples, is shown when comparing the control and scaffold group with this statistical model.

The measurements of mineralised bone tissue, expressed in percentages, are shown in Table 2.

Follow-up	Mineralised Area
4 w	~10%
12 w	~30%
24 w	~60%

Table 2: Percentage of defect's surface with bone mineralization at 4, 12 and 24 weeks.

Histological analysis

Comparison of samples taken at 4 and 12 weeks shows the following: the untreated defect is rich in fibrous tissue partially infiltrated by bone tissue at the periphery (Figure 14A-B). The scaffold-treated defect is occupied by new bone tissue and partially by fibrous tissue undergoing mineralization (Figure 14C-D).

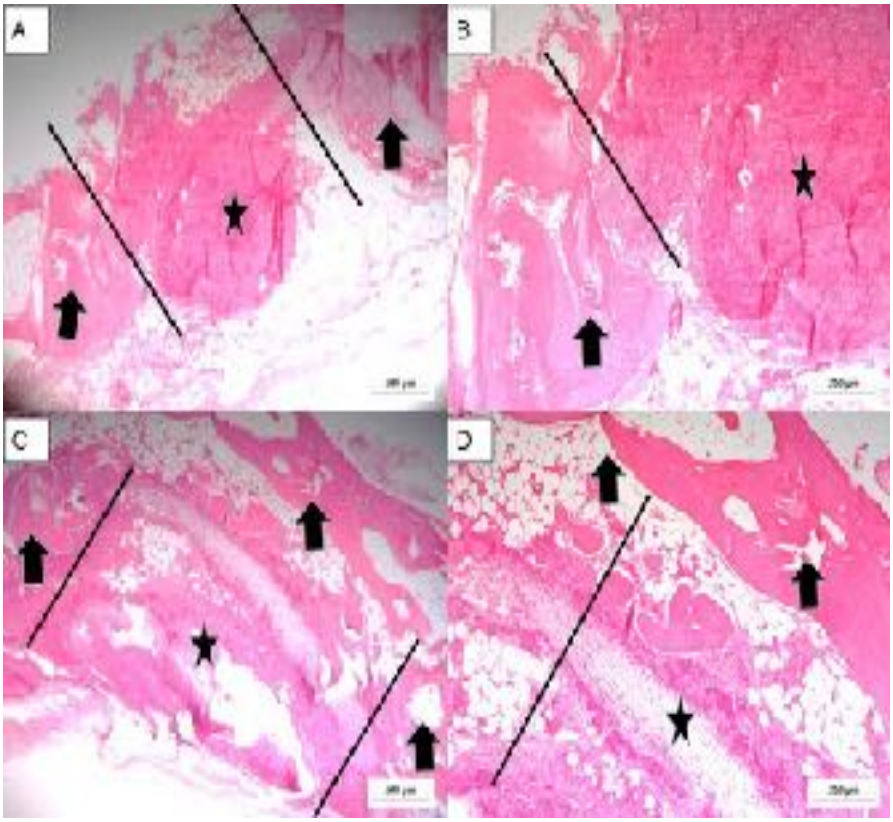

Figure 14: A-B: Hematoxylin and eosin stain of untreated bone defect 4 weeks post implant (magnification: A: 2,5X – B: 5X). C-D: Hematoxylin and eosin stain of treated bone defect 12 weeks post implant (magnification: C: 2,5X – D: 5X). The bone defect is located between the parallel bars.

Macroscopically, the sample analysed at 24 weeks shows two partially healed defects in both the control and the scaffold-treated defect. However, in each case there is a reduction in parietal thickness.

The haematoxylin-eosin sections show the following. An area of bone remodelling is evident in the untreated defect. Poorly mineralised, thinned and fragmented trabeculae with numerous areas of osteonecrosis are

visible (Figure 15a). The medullary cavities show exclusively adipose marrow.

The scaffold-treated defect, on the other hand, shows not only areas of osteonecrosis with thinned and poorly mineralised bone lamellae, but also multiple areas of osteosynthesis with evidence of immature bone tissue in formation and numerous activated osteoblasts (Figure 15b). There are also fragments of birefringent amorphous material, which may be scaffold residues (Figure 15c). Residual medullary cavities with clearly visible haemopoietic niches are also present (Figure 15d). No inflammatory infiltrates of any kind are evident.

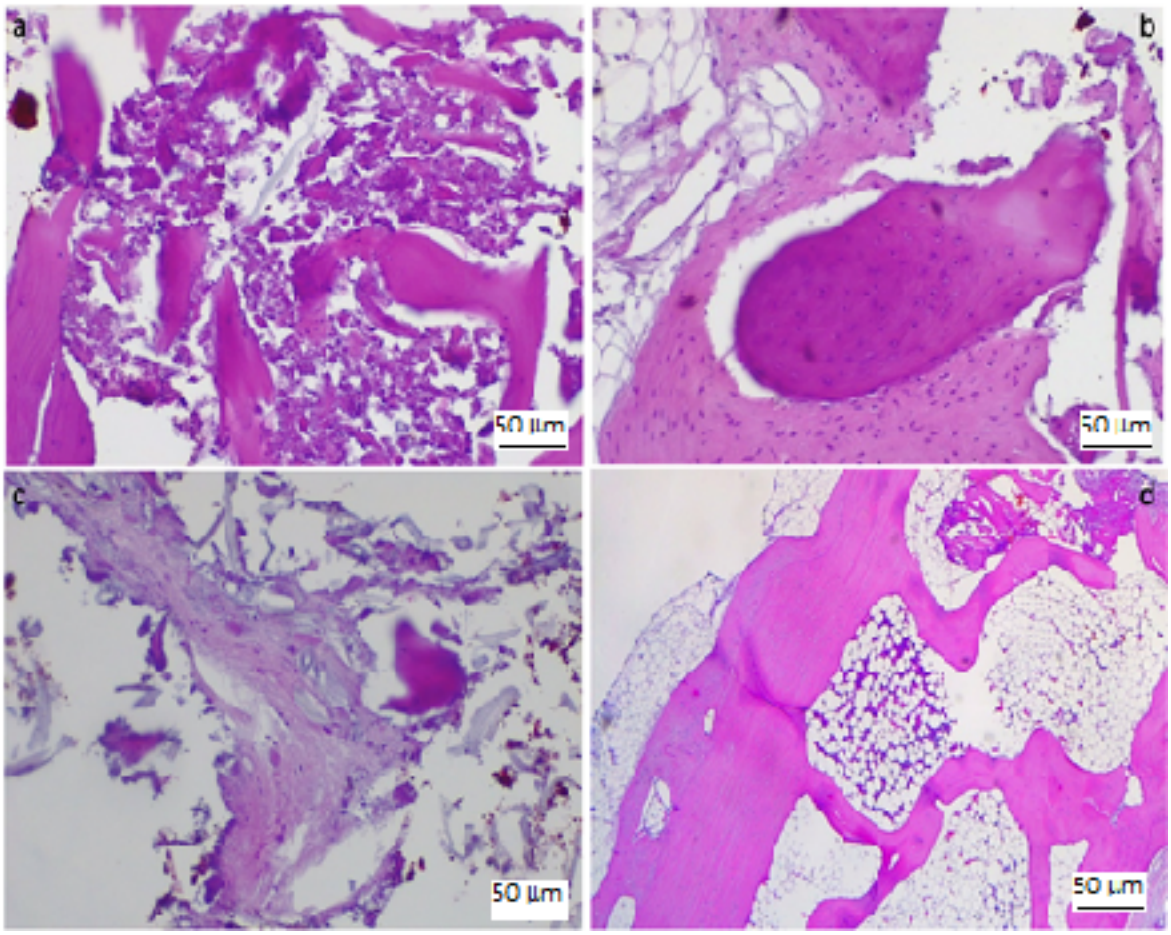

Figure 15 : a) Osteonecrosis in hematoxylin and eosin stain of treated bone defect 24 weeks post implant (magnification: 20X); b) Bone deposition and necrotic bone fragments in hematoxylin and eosin stain of treated bone defect 24 weeks post implant (magnification: 20X); c) Periosseous tissue with embedded amorphous fragments (scaffold); d) Bone marrow with hematopoietic stem cell niches.

Immunohistochemical staining for CD56 (Figure 16) shows that areas of osteosynthesis are more represented in the scaffold-treated samples. Furthermore, the density of osteoblasts detected in these areas is higher than in the control samples. Specimens of the control group have more areas of necrosis and fibrosis. Therefore, the evaluation of the CD56 marker in samples left to spontaneous healing is non-specific. In both tissues, control and scaffold, analysis with CD34 and CD68 markers reveals the following: a normal microvascular density, the percentage of haematopoietic precursor cells <2% and osteoclastic component was not increased. Therefore, evaluation with CD68 and CD34 shows no relevant results.

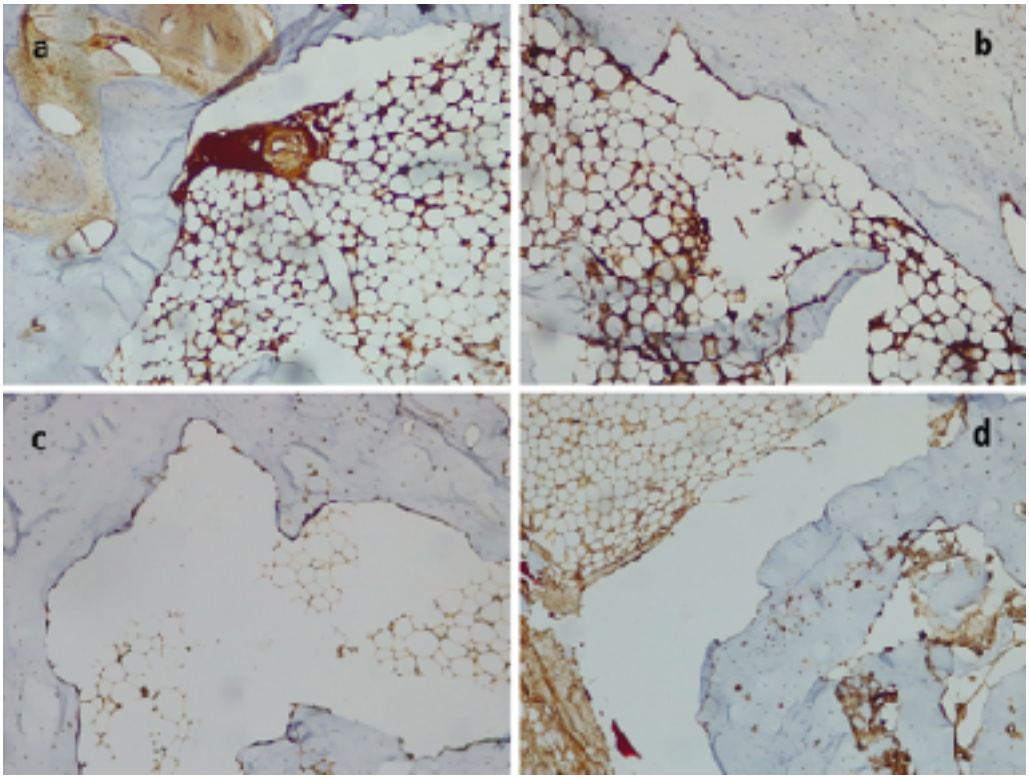

Figure 16: The immunohistochemical marker CD56 shows activated osteoblasts at 24 weeks after implantation in the scaffold-treated samples (a, b) and the control group (c, d). 10x magnification.

Complications

The study does not show any specific complications related to the scaffold or involving rabbits.

Part Two: Tibia

Scaffold

The morphology of the scaffold appears as a sheet of intertwined fibers, with a diameter of the fibers varies from a minimum of 150 nm to a maximum of 650 nm (Figure 17, 18). Hydroxyapatite nanoparticle are also visible in the SEM image and computed Xray-microtomography (microCT). The scaffold has an average thickness of about 2.5 mm (measured by microCT, Figure 19) and sufficient rigidity for handling during implantation.

A manually cut 8 mm diameter circular scaffold was realized, customized to be implanted in rabbit bone defect.

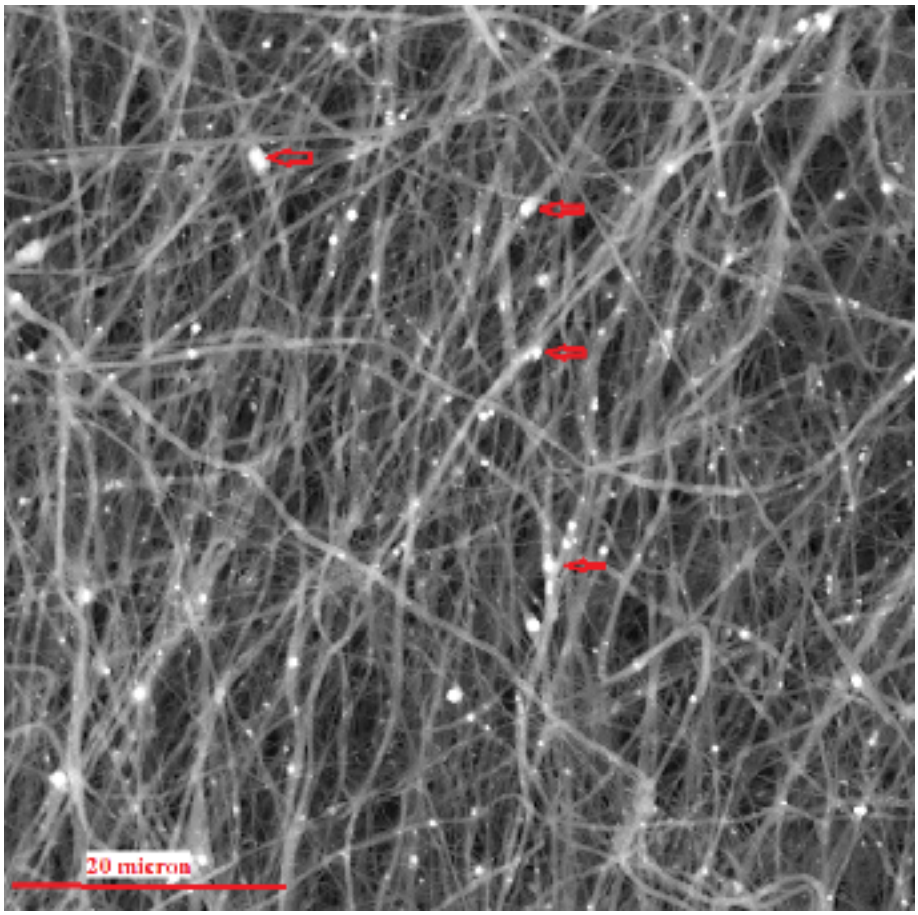

Figure 17: SEM image of electrospun PBS scaffold at 4000x magnification. Red arrows of image at left indicate hydroxyapatite nanoparticles.

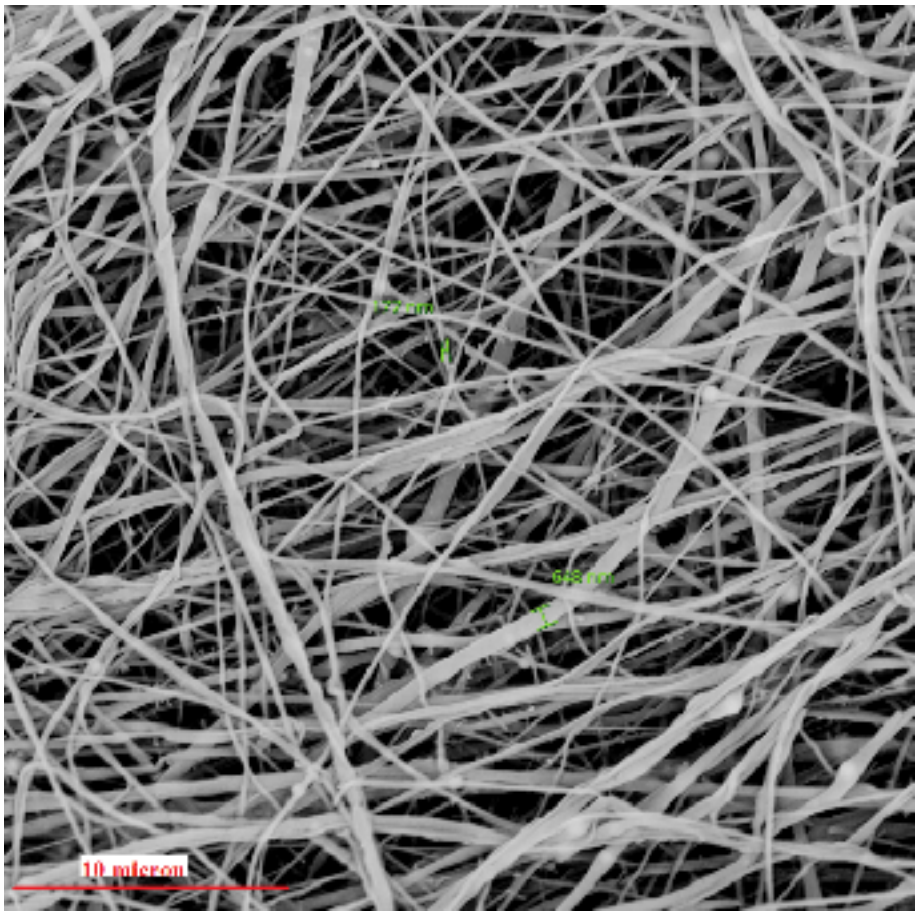

Figure 17: SEM image of electrospun PBS scaffold at 8000x magnification. Red arrows of image at left indicate hydroxyapatite nanoparticles.

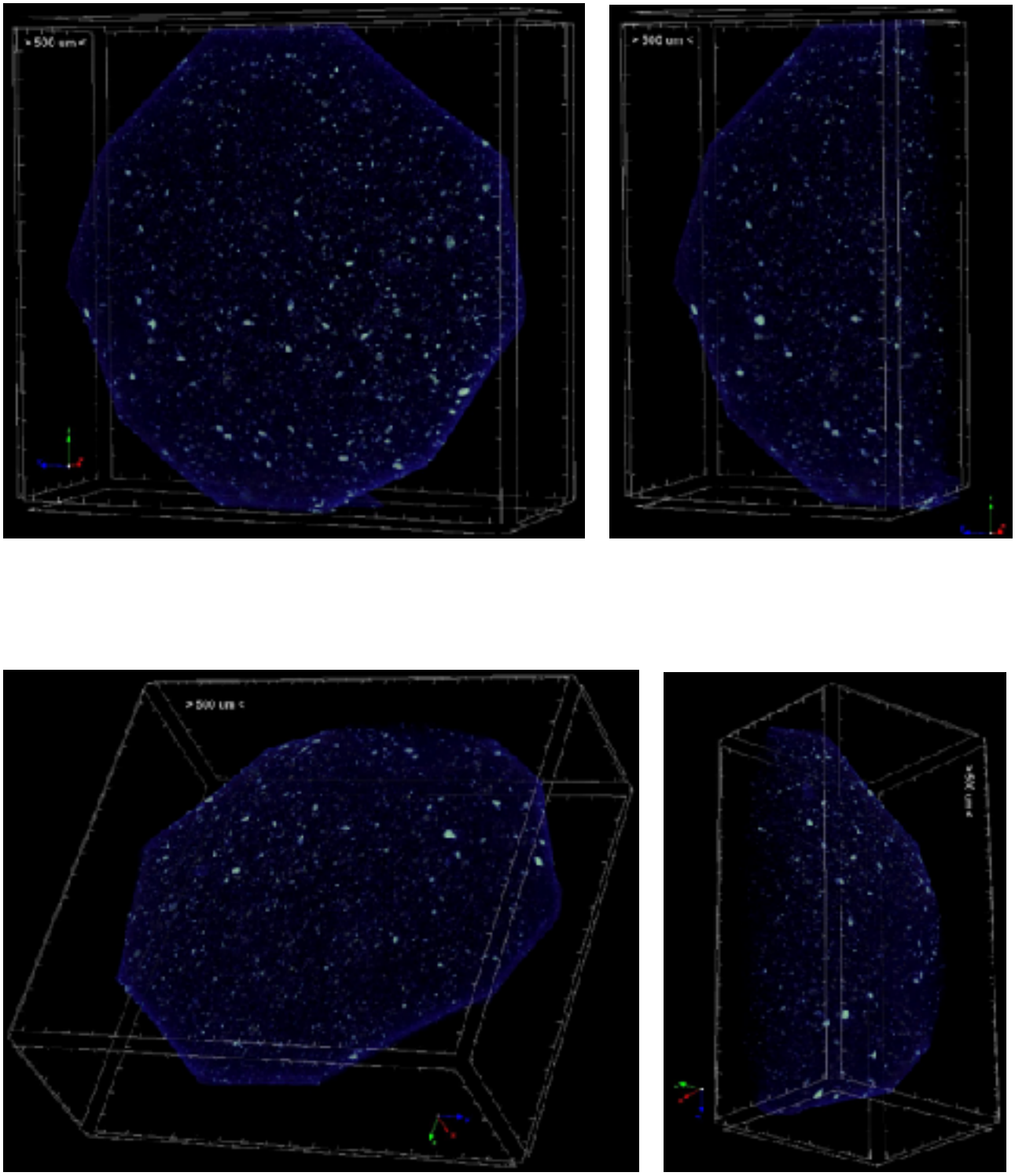

Figure 18: microCT reconstruction of PBS scaffold. White spots are hydroxyapatite nanoparticles.

Histological analysis

The control group sample analysed at 24 weeks shows only partial filling of the tibial defect. The areas of newly formed bone tissue are scarce and not always observable (Figure 19).

The tibial defect treated with the protein-printed scaffold (group A) shows, in addition to some areas of osteonecrosis with thinned and poorly mineralised bone lamellae, multiple areas of osteosynthesis with evidence of immature bone tissue in formation and numerous activated osteoblasts (Figure 20).

Group B samples, whose defect is treated with protein-impregnated scaffold, show only limited calcification of the scaffold (Figure 21).

However, in both A and B groups, the presence of amorphous material at the tibial defect was still evident, as the scaffold is not completely degraded at this stage.

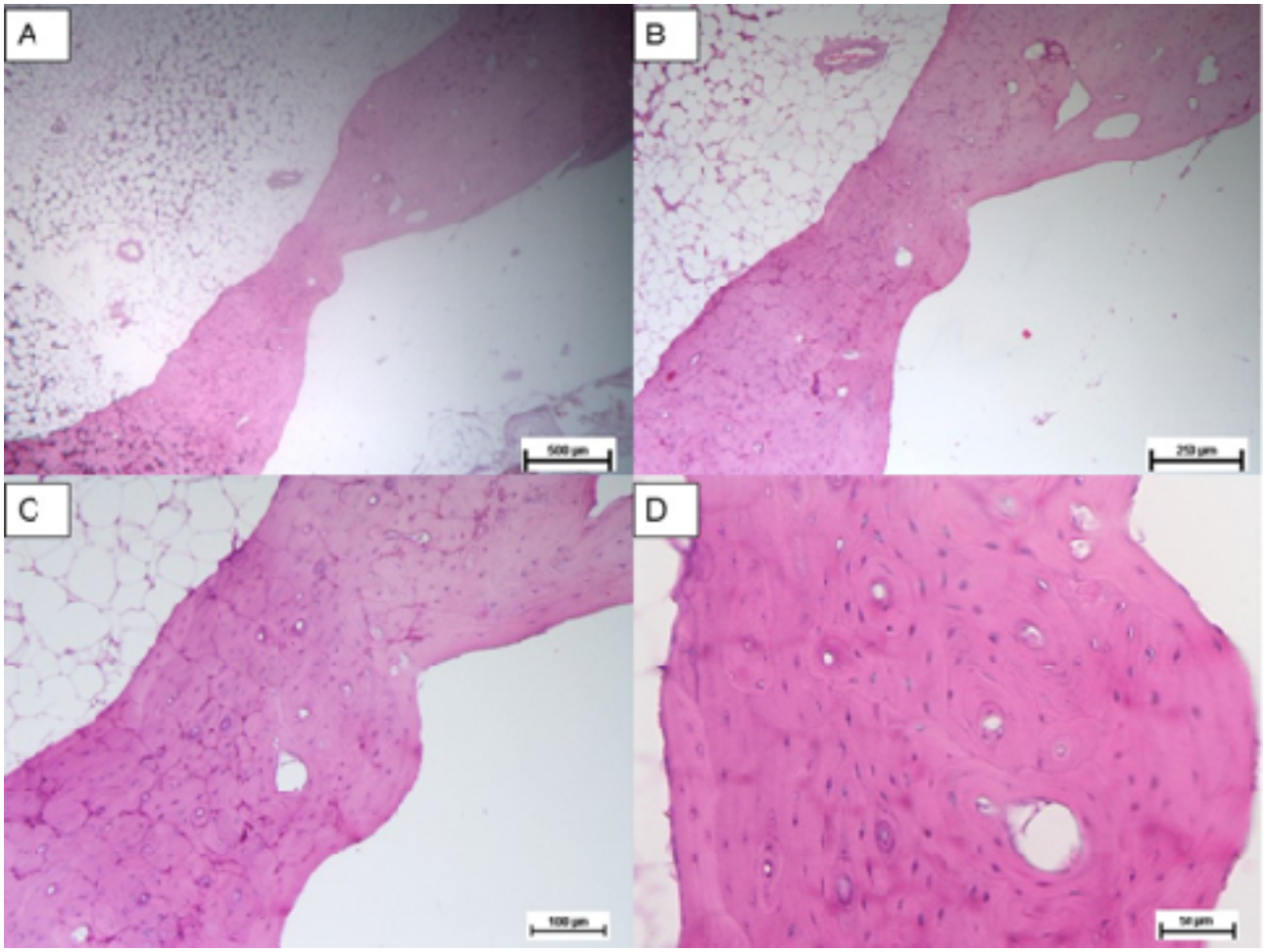

Figure 19: Control group A-B: Hematoxylin and eosin stain of untreated bone defect; tibial defect (star). Magnification: A: 2,5X, B: 5X, C:10X, D: 20X.

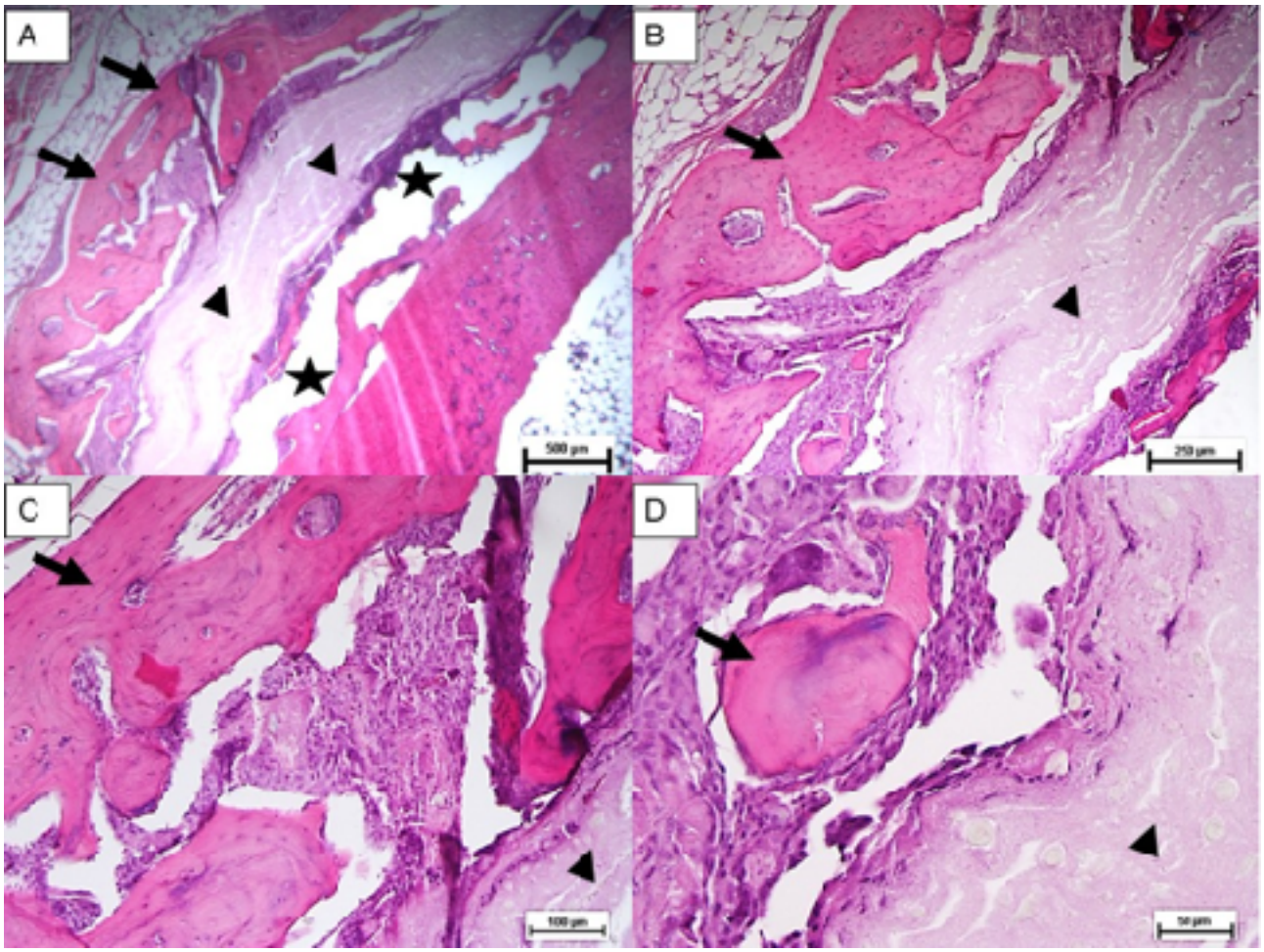

Figure 20: Group A: Hematoxylin and eosin stain of treated bone defect with the printed protein scaffold. New bone area (Arrow); scaffold (arrowhead); tibial defect (star). Magnification: A: 2,5X, B: 5X, C:10X, D: 20X.

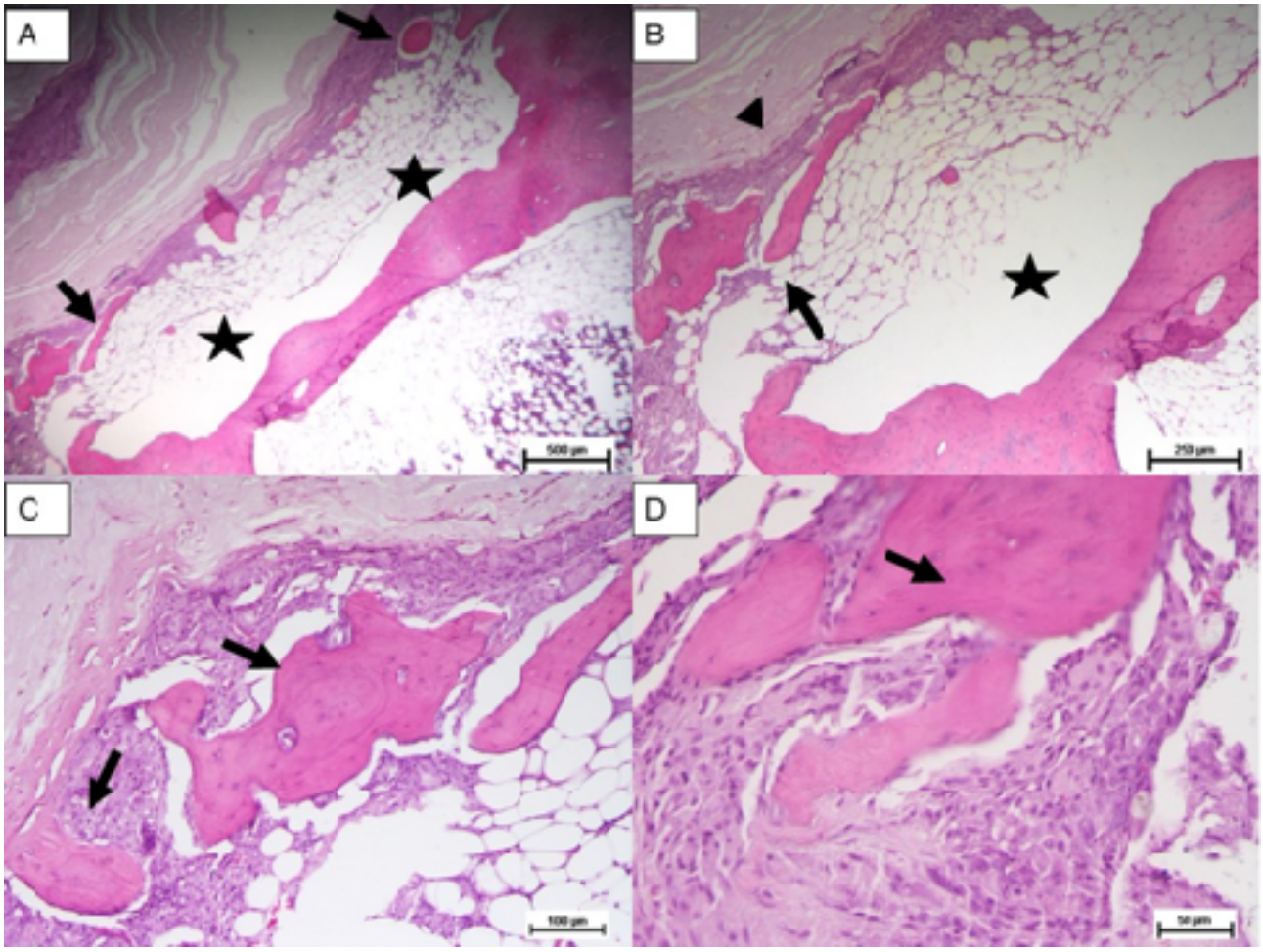

Figure 21: Group B: Hematoxylin and eosin stain of treated bone defect with the impregnated protein scaffold. New bone area (Arrow); scaffold (arrowhead); tibial defect (star). Magnification: A: 2,5X, B: 5X, C:10X, D: 20X.

Complications

Upon excision of the specimens, macroscopic observation of the samples shows a significant difference in the bone profile (Figure 22). The formation of hypertrophic callus or heterotopic bone is to be identified as a complication. However, the animals do not show any health problems in general or related to the implant area. The periosteal tissue, still present in the photos in Figure 22, also shows no alteration. Furthermore, the histological examination shows no significant alterations.

Figure 22: Photo of the harvest of the specimens before incision of the periosteal tissue. The absence of alteration of the bone profile in the control group can be seen in the picture on the left. The formation of hypertrophic callus or heterotopic bone can be observed in the study groups, Group A in the centre and Group B on the right.

CHAPTER 4

Discussion

For the first time, in a rabbit animal model, this project demonstrates that a micro-fibrillar PBS scaffold is effective in improving bone regeneration in critical bone defects.

The first part of the project also demonstrates the absence of adverse events, thus confirming the biocompatibility and biodegradability of the PBS scaffold. After the application of the device on the rabbit's cranial theca, the second part of the project shows the applicability of the scaffold also on the tibia, a long bone. Furthermore, for the first time, a scaffold is created in PBS with hydroxyapatite and ciprofloxacin and engineered with BMP-2. Therefore, this study demonstrates the enormous potential of PBS scaffolds applied to bone tissue. The device designed and studied in this project also demonstrates easy applicability as a surgical device, without intra- or post-operative complications.

The first part of the study, on the cranial theca, is crucial as it demonstrates the applicability of the scaffold to bone tissue. From a surgical point of view, there were no significant challenges in implanting the device. In addition, histological examinations and imaging studies performed in serial follow-ups make it possible to exclude adverse reactions that may affect the health of the animals. All these evaluations make it possible to reduce the number of animals used in the second part of the project, which is crucial for identifying the best engineering method with BMP-2 and laying the foundations for larger studies. Radiological evaluation by CT examination shows incomplete healing in both untreated and scaffold-

treated defects. However, as in similar studies [36,37], significant differences are only observed as an assessment of the area of mineralised tissue. Statistical analysis based on the measurement of defect diameter defines bone regeneration as significant in the intervals between 0 and 24 weeks, 4 and 24 weeks and 12 and 24 weeks in the entire population. This evidence is essential to exclude any negative effects of scaffold application on bone tissue. However, limited healing is observed in both defects in the first four weeks. Thus, if analysed with this method, the scaffold does not seem to offer a clear advantage. Histological evaluation, performed on bone sections of the defect, reveals important information. In all samples, signs of inflammatory infiltrates around the scaffold are absent, which confirms the biocompatibility and biodegradability of the material. Thus, even in a different tissue type, the biocompatibility and biodegradability of 3D PBS-based scaffolds are confirmed [33].

Furthermore, histological analysis shows that an increased infiltration of mineralised tissue is present with scaffold implantation. This, unlike the control, involves almost the entire surface of the defect. It is important to note that these results are progressive in subsequent follow-ups. An infiltration of bone tissue with greater amounts of mineralised tissue compares favourably with a majority of fibrous tissue in controls. Another relevant factor in scaffold-treated defects is the presence of periosteal fibrous tissue, which is indicative of florid osteosynthesis.

Immunohistochemical analysis is not indicative for CD 68 and CD34 while it shows important evidence for CD56. Also known as NCAM (Neural Cell Adhesion Molecule), CD56 is a glycoprotein that plays a crucial role in cell adhesion and cell-cell interactions. In the context of bone regeneration, CD56 is a useful marker to identify the activated osteoblast cell, a key element in bone tissue regeneration. The results of the study group show a marked positivity for CD56 at the transition point between healthy bone and the ‘fracture zone’, thus indicating a well-initiated bone regeneration process. The finding of haemopoietic niches in the same areas is also indicative of increased bone maturation. The immunohistochemical analysis shows other positive evidence. In the scaffold-treated specimens, the areas of osteosynthesis are much more represented than in the control group. Furthermore, in these areas the density of osteoblasts detected is higher than in the control samples, in which the total number of osteoblasts is lower. Finally, the control specimens, left to heal spontaneously, have more areas of necrosis and fibrosis, in which the marker evaluation shows non-specific characterisation. Thus, although there is no statistically significant evidence of faster defect healing by imaging, the histological study shows a significant qualitative advantage in scaffold-treated defects. Furthermore, the normal density of haematopoietic precursor cells, osteoclastic component and microvascular density indicates that the scaffold did not alter any of these processes.

Considering these results as very promising, the study proceeds with the realisation of the engineered scaffolds.

The second part of the study is performed with a small number of animals in order to identify the most suitable scaffold engineering model and to validate the choice of growth factor and antibiotic. The difference in the bone profile in the Group A and B samples shown in Figure 22 is objective. The study group, regardless of the protein addition method, shows a reaction such as a hypertrophic callus or heterotopic bone formation. As described in the literature, this is attributable to the use of supra-physiological doses of BMP-2. At this pre-clinical stage, it is difficult to determine how relevant this effect is. However, histological analysis shows increased bone regeneration in the study group samples. Specifically, the scaffold with printed protein (Group A) shows a considerably greater amount of osteosynthesis areas and activated osteoblasts than Group B. Therefore, the main result of this second part of the study is to have identified the scaffold with printed protein as the device with the greatest potential.

The search for a scaffold with osteogenic and osteoinductive properties finds ample space in the literature. Other studies show similar results to those described in this study, although it is almost impossible to compare the studies with each other in terms of results. Also, in an animal model of a rabbit with a radial defect, a Chinese research group demonstrated similar properties by achieving the osteogenic effect with osteoinductive

periosteum mimetic [12]. A similarity can also be found in the study design used to validate the scaffold properties. For example, Teotia et al. also studied their scaffolds, of 3D-printed porous composite structure with resins and osteoinductive growth factors, on both flat bone (cranial theca) and long bone (tibia) [15]. Hwan D Kim's research group showed that increasing the local concentration of phosphate ions in their scaffolds promotes the activation of transcription factors, such as osteocalcin and osteopontin, which induce osteogenic differentiation in stem cells [13]. This is the goal of all scaffolds with osteoinductive characteristics. In this project, PBS is studied for the first time. This material proves to be a biocompatible material in the first part of the project. The production of the scaffold by electrospinning with a micro-fibrillar structure and the entire manufacturing process is another objective of this study. The manufacturing process of the scaffold is probably a crucial factor in the osseointegration process. Electrospinning allows the fabrication of fibres with a variable diameter down to the nanometre range by exploiting electrostatic forces generated by a high potential difference between two electrodes [38]. The intention is to artificially generate a scaffold that mimics the characteristics of the extracellular matrix, triggering the growth of osteoblastic cells, which is then further enhanced by BMP-2. Haider et al. had well explained the intent in an in vitro study where BMP-2 was added to a hydroxyapatite (HA) and Poly(L-lactide-co-glycolide) (PLGA) nanofibre scaffold [39].

In 2018, Preethi Soundarya et al. provided an overview of different fabrication techniques for scaffold production but, concluded that an ideal production method for a scaffold has not yet been determined. Therefore, considering the results of the current study, the author believes that the micro-fibrillar PBS scaffold produced by electrospinning may be a viable alternative to those proposed in the current literature.

In addition, the biomechanical characteristics of the scaffold produced in this study also allow its easy surgical applicability in both phases of the project. This feature is of fundamental importance in a study with translational objectives, towards surgery on humans.

Another crucial aspect in this area concerns the complexity of scaffold production processes. These devices, especially engineered ones, require the use of highly sophisticated technologies and expensive materials that are often difficult to obtain. All tissue engineering and regenerative medicine has the ultimate goal of working on a large scale. Although several studies show encouraging results, in all of them the production aspect is limited to a very few devices produced in highly specialised facilities and at considerable cost. Therefore, although the potential of these scaffolds is considerable, it is unlikely that they will be adopted on a large scale any time soon, as their widespread use requires further technological development and reductions in production costs.

The main limitation of the study is the small number of samples. This limits the effectiveness of the statistical analysis, but at the same time it must

also comply with legislative limitations. The CT evaluation, even if used as a reference in other studies, has limitations due to its method of execution and precision.

The future implications of this study are significant. The second part of the study already sets the goal of testing the printed scaffold on a number of cases congruent for statistical significance. The validation of the properties of the PBS scaffold as a carrier structure for osteoinductive growth factors leaves room for the possibility of testing additional or alternative molecules. Furthermore, the future goal of this project is to produce a scaffold that is effective not only on bone tissue and its critical defects, but also at the interface between bone and tendon. This area represents perhaps one of the greatest interests in terms of numbers for orthopaedic surgery.

Finally, for future perspectives in this field, the most innovative is looking at microRNAs. Arriaga, et al. [40], have already achieved positive results in 2019, both in terms of bone regeneration and vascularisation. Therefore, future studies could also focus on devices created to directly deliver miRNAs or anti-miRNAs into cells in vivo. Especially in this case, however, it is necessary to consider how the production and economic factors are not negligible.

CHAPTER 5

Conclusion

In a rabbit animal model, this study demonstrates, for the first time, that a micro-fibrillar PBS scaffold is effective in improving bone regeneration in critical bone defects. The absence of adverse events demonstrates the scaffold's biocompatibility and biodegradability properties. In the first part of the project, histological and immunohistochemical evaluation demonstrates a clear qualitative improvement in bone regeneration compared to spontaneous healing. Therefore, the PBS micro-fibrillar scaffold made in this study has osseointegration capacity and osteogenic action. For the second part of the project, a PBS scaffold with hydroxyapatite and ciprofloxacin and further engineered with BMP-2 is made for the first time. The scaffold thus created demonstrates its applicability in bone tissue, in this case the tibia, a long bone. Furthermore, the scaffold made with the printed protein proves to be the most effective in enhancing osteoinductive activity compared to the other model and the control group left to heal spontaneously. Finally, from a surgical point of view, the device designed and studied in this project demonstrates excellent biomechanical characteristics, with easy applicability during surgery and no intra- or post-operative complications.

CHAPTER 6

References

1. Sen M, Miclau T. Autologous iliac crest bone graft: should it still be the gold standard for treating nonunions? Injury. 2007;38(Suppl 1):S75–80. doi: 10.1016/ j.injury.2007.02.012.

2. Kong L, Ao Q, Wang A, Gong K, Wang X, Lu G, Gong Y, Zhao N, Zhang X. Preparation and characterization of a multilayer biomimetic scaffold for bone tissue engineering. J Biomater Appl. 2007 Nov;22(3):223-39. doi: 10.1177/0885328206073706. Epub 2007 Jan 25. PMID: 17255157.

3. Preethi Soundarya S, Haritha Menon A, Viji Chandran S, Selvamurugan N. Bone tissue engineering: Scaffold preparation using chitosan and other biomaterials with different design and fabrication techniques. Int J Biol Macromol. 2018 Nov;119:1228-1239. doi: 10.1016/j.ijbiomac.2018.08.056. Epub 2018 Aug 11. PMID: 30107161.

4. Yang D, Xiao J, Wang B, Li L, Kong X, Liao J. The immune reaction and degradation fate of scaffold in cartilage/bone tissue engineering. Mater Sci Eng C Mater Biol Appl. 2019 Nov;104:109927. doi: 10.1016/j.msec.2019.109927. Epub 2019 Jun 28. PMID: 31500038.

5. Algul D, Sipahi H, Aydin A, Kelleci F, Ozdatli S, Yener FG. Biocompatibility of biomimetic multilayered alginate-chitosan/β-TCP scaffold for osteochondral tissue. Int J Biol Macromol. 2015 Aug;79:363-9. doi: 10.1016/j.ijbiomac.2015.05.005. Epub 2015 May 14. PMID: 25982954.

6. Lee SH, Lee KG, Hwang JH, Cho YS, Lee KS, Jeong HJ, Park SH, Park Y, Cho YS, Lee BK. Evaluation of mechanical strength and bone regeneration ability of 3D printed kagome-structure scaffold using rabbit calvarial defect model. Mater Sci Eng C Mater Biol Appl. 2019 May;98:949-959. doi: 10.1016/j.msec.2019.01.050. Epub 2019 Jan 14. PMID: 30813102.

7. Lim JX, He M, Chong AKS. 3D-printed Poly-Lactic Co-Glycolic Acid (PLGA) scaffolds in non-critical bone defects impede bone regeneration in rabbit tibia bone. Biomed Mater Eng. 2021;32(6):375-381. doi: 10.3233/BME-216017. PMID: 34633315.

8. Maeda NT, Yoshimoto M, Allegrini S Jr, Bressiani AH. Hydroxyapatite Dome for Bone Neoformation in Rabbit Tibia. Int J Oral Maxillofac Implants. 2016 May-Jun;31(3):571-9. doi: 10.11607/jomi.4412. PMID: 27183066.

9. Ma J, Wu S, Liu J, Liu C, Ni S, Dai T, Wu X, Zhang Z, Qu J, Zhao H, Zhou D, Zhao X. Synergistic effects of nanoattapulgite and hydroxyapatite on vascularization and bone formation in a rabbit tibia bone defect model. Biomater Sci. 2022 Aug 9;10(16):4635-4655. doi: 10.1039/d2bm00547f. PMID: 35796642.

10. Lin H, Li Z, Xie Z, Tang S, Huang M, Feng J, Wei Y, Shen Z, Zhou R, Feng Y, Chen H, Ren Y, Huang F, Wang X, Jiang Z. An anti-infection and biodegradable TFRD-loaded porous scaffold promotes bone regeneration in segmental bone defects: experimental studies. Int J Surg. 2024 Jun 1;110(6):3269-3284. doi: 10.1097/JS9.0000000000001291. PMID: 38506734; PMCID: PMC11175727.

11. Ray S, Nandi SK, Dasgupta S. Enhanced bone regeneration usingAntheraea mylittasilk fibroin and chitosan based scaffold:in-vivoandin-vitrostudy. Biomed Mater. 2023 Aug 18;18(5). doi: 10.1088/1748-605X/acee3c. PMID: 37552994.

12. Guo HG, Yao FL, Ma XL, Yao KD. [An experimental study on rabbit's radial bone defect healed by application of mimetic periosteum with tissue-engineered bone]. Zhonghua Zheng Xing Wai Ke Za Zhi. 2008 Jan;24(1):63-7. Chinese. PMID: 18437989.

13. Kim HD, Amirthalingam S, Kim SL, Lee SS, Rangasamy J, Hwang NS. Biomimetic Materials and Fabrication Approaches for Bone Tissue Engineering. Adv Healthc Mater. 2017 Dec;6(23). doi: 10.1002/adhm.201700612. Epub 2017 Nov 24. PMID: 29171714.

14. Pförringer D, Harrasser N, Beirer M, Crönlein M, Stemberger A, van Griensven M, Lucke M, Burgkart R, Obermeier A. Influence of Absorbable Calcium Sulfate-Based Bone Substitute Materials on Human Haemostasis-In Vitro Biological Behavior of Antibiotic Loaded Implants. Materials (Basel). 2018 Jun 1;11(6):935. doi: 10.3390/ma11060935. PMID: 29865173; PMCID: PMC6025628.

15. Teotia AK, Dienel K, Qayoom I, van Bochove B, Gupta S, Partanen J, Seppälä J, Kumar A. Improved Bone Regeneration in Rabbit Bone Defects Using 3D Printed Composite Scaffolds Functionalized with Osteoinductive Factors. ACS Appl Mater Interfaces. 2020 Oct 28;12(43):48340-48356. doi: 10.1021/acsami.0c13851. Epub 2020 Oct 13. PMID: 32993288.

16. Kalay E, Ermutlu C, Yenigül AE, Yalçınkaya U, Sarısözen B. Effect of bone morphogenic protein-2 and desferoxamine on distraction osteogenesis. Injury. 2022 Jun;53(6):1854-1857. doi: 10.1016/j.injury.2022.03.064. Epub 2022 Apr 1. PMID: 35410738.

17. Ducy P, Karsenty G. The family of bone morphogenetic proteins. Kidney Int 2000;57(6):2207–14. doi:10.1046/j.1523-1755.2000.00081.x.

18. Mai Z, Peng Z, Wu S, Zhang J, Chen L, Liang H, et al. Single bout short du- ration fluid shear stress induces osteogenic differentiation of MC3T3-E1 cells via integrin β1 and BMP2 signaling cross-talk. PLoS ONE 2013;8(4):e61600. doi:10.1371/ journal.pone.0061600.

19. Moutsatsos IK, Turgeman G, Zhou S, Kurkalli BG, Pelled G, Tzur L, Kelley P, Stumm N, Mi S, Müller R, Zilberman Y, Gazit D. Exogenously regulated stem cell-mediated gene therapy for bone regeneration. Mol Ther 2001;3(4):449– 61. doi:10.1006/ mthe.2001.0291.

20. Ripamonti U, Crooks J, Matsaba T, Tasker J. Induction of endochondral bone formation by recombinant human transforming growth factor-beta2 in the baboon (Papio ursinus). Growth Factors 2000;17(4):269–85. doi:10.3109/ 08977190009028971.

21. Chen D, Zhao M, Mundy GR. Bone morphogenetic proteins. Growth Factors. 2004 Dec;22(4):233-41. doi: 10.1080/08977190412331279890. PMID: 15621726.

22. James AW, LaChaud G, Shen J, Asatrian G, Nguyen V, Zhang X, Ting K, Soo C. A Review of the Clinical Side Effects of Bone Morphogenetic Protein-2. Tissue Eng Part B Rev. 2016 Aug;22(4):284-97. doi: 10.1089/ten.TEB.2015.0357. Epub 2016 Apr 19. PMID: 26857241; PMCID: PMC4964756.

23. Lee S, Kang BJ. Surgical Reconstruction of Canine Nonunion Fractures Using Bone Morphogenetic Protein-2-loaded Alginate Microbeads and Bone Allografts. In Vivo. 2024 Mar-Apr;38(2):611-619. doi: 10.21873/invivo.13480. PMID: 38418118; PMCID: PMC10905487.

24. Kurien T, Pearson RG, Scammell BE. Bone graft substitutes currently available in orthopaedic practice: the evidence for their use. Bone Joint J. 2013 May;95-B(5):583-97. doi: 10.1302/0301-620X.95B5.30286. PMID: 23632666.

25. Jégoux F, Goyenvalle E, Cognet R, Malard O, Moreau F, Daculsi G, Aguado E. Mandibular segmental defect regenerated with macroporous biphasic calcium phosphate, collagen membrane, and bone marrow graft in dogs. Arch Otolaryngol Head Neck Surg. 2010 Oct;136(10):971-8. doi: 10.1001/archoto.2010.173. PMID: 20956742.

26. Han SH, Cha M, Jin YZ, Lee KM, Lee JH. BMP-2 and hMSC dual delivery onto 3D printed PLA-Biogel scaffold for critical-size bone defect regeneration in rabbit tibia. Biomed Mater. 2020 Dec 12;16(1):015019. doi: 10.1088/1748-605X/aba879. PMID: 32698169.

27. Go YY, Mun JY, Chae SW, Kim SH, Song H, Song JJ. Engineering functional BMP-2 expressing teratoma-derived fibroblasts for enhancing osteogenesis. Sci Rep.

2018 Oct 1;8(1):14581. doi: 10.1038/s41598-018-32946-6. PMID: 30275449; PMCID: PMC6167319.

28. Yoon SJ, Yoo Y, Nam SE, Hyun H, Lee DW, Um S, Kim SY, Hong SO, Yang DH, Chun HJ. The Cocktail Effect of BMP-2 and TGF-β1 Loaded in Visible Light-Cured Glycol Chitosan Hydrogels for the Enhancement of Bone Formation in a Rat Tibial Defect Model. Mar Drugs. 2018 Sep 25;16(10):351. doi: 10.3390/md16100351. PMID: 30257482; PMCID: PMC6213427.

29. Saninggar KE, Abe F, Nakano A, Kato K. Collagen-binding bone morphogenetic protein-2 designed for use in bone tissue engineering. Dent Mater J. 2024 Sep 28;43(5):718-728. doi: 10.4012/dmj.2024-138. Epub 2024 Aug 30. PMID: 39218686.

30. Edelmayer M, Wehner C, Ulm C, Zechner W, Shafer D, Agis H. Which substances loaded onto collagen scaffolds influence oral tissue regeneration?-an overview of the last 15 years. Clin Oral Investig. 2020 Oct;24(10):3363-3394. doi: 10.1007/s00784-020-03520-0. Epub 2020 Aug 22. PMID: 32827278.

31. Rico-Llanos GA, Borrego-González S, Moncayo-Donoso M, Becerra J, Visser R. Collagen Type I Biomaterials as Scaffolds for Bone Tissue Engineering. Polymers (Basel). 2021 Feb 17;13(4):599. doi: 10.3390/polym13040599. PMID: 33671329; PMCID: PMC7923188.

32. Kalay E, Ermutlu C, Yenigül AE, Yalçınkaya U, Sarısözen B. Effect of bone morphogenic protein-2 and desferoxamine on distraction osteogenesis. Injury. 2022 Jun;53(6):1854-1857. doi: 10.1016/j.injury.2022.03.064. Epub 2022 Apr 1. PMID: 35410738.

33. Cicero, L., Licciardi, M., Cirincione, R., Puleio, R., Giammona, G., Giglia, G., Sardo, P., Edoardo Vigni, G., Cioffi, A., Sanfilippo, A., & Cassata, G. (2021). Polybutylene succinate artificial scaffold for peripheral nerve regeneration. Journal of Biomedical

Materials Research Part B: Applied Biomaterials, 1– 10. https://doi.org/10.1002/jbm.b.34896

34. Ojansivu M, Johansson L, Vanhatupa S, Tamminen I, Hannula M, Hyttinen J, Kellomäki M, Miettinen S. Knitted 3D Scaffolds of Polybutylene Succinate Support Human Mesenchymal Stem Cell Growth and Osteogenesis. Stem Cells Int. 2018 May 7;2018:5928935. doi: 10.1155/2018/5928935. PMID: 29853915; PMCID: PMC5964421.

35. Mochane MJ, Magagula SI, Sefadi JS, Mokhena TC. A Review on Green Composites Based on Natural Fiber-Reinforced Polybutylene Succinate (PBS). Polymers (Basel). 2021 Apr 8;13(8):1200. doi: 10.3390/polym13081200. PMID: 33917740; PMCID: PMC8068185.

36. Pihlman H, Keränen P, Paakinaho K, Linden J, Hannula M, Manninen IK, Hyttinen J, Manninen M, Laitinen-Vapaavuori O. Novel osteoconductive β-tricalcium phosphate/poly(L-lactide-co-e-caprolactone) scaffold for bone regeneration: a study in a rabbit calvarial defect. J Mater Sci Mater Med. 2018 Oct 8;29(10):156. doi: 10.1007/s10856-018-6159-9. PMID: 30298429.

37. Pfau MR, Beltran FO, Woodard LN, Dobson LK, Gasson SB, Robbins AB, Lawson ZT, Brian Saunders W, Moreno MR, Grunlan MA. Evaluation of a self-fitting, shape memory polymer scaffold in a rabbit calvarial defect model. Acta Biomater. 2021 Dec;136:233-242. doi: 10.1016/j.actbio.2021.09.041. Epub 2021 Sep 24. PMID: 34571270; PMCID: PMC8742656.

38. Wang Z, Wang Y, Yan J, Zhang K, Lin F, Xiang L, Deng L, Guan Z, Cui W, Zhang H. Pharmaceutical electrospinning and 3D printing scaffold design for bone regeneration. Adv Drug Deliv Rev. 2021 Jul;174:504-534. doi: 10.1016/j.addr.2021.05.007. Epub 2021 May 13. PMID: 33991588.

39. Haider A, Kim S, Huh MW, Kang IK. BMP-2 Grafted nHA/PLGA Hybrid Nanofiber Scaffold Stimulates Osteoblastic Cells Growth. Biomed Res Int. 2015;2015:281909. doi: 10.1155/2015/281909. Epub 2015 Oct 11. PMID: 26539477; PMCID: PMC4619782.

40. Arriaga MA, Ding MH, Gutierrez AS, Chew SA. The Application of microRNAs in Biomaterial Scaffold-Based Therapies for Bone Tissue Engineering. Biotechnol J. 2019 Oct;14(10):e1900084. doi: 10.1002/biot.201900084. Epub 2019 Jul 9. PMID: 31166084.

Acknowledgements

A special acknowledgement goes to Dr. Luca Cicero (IZS Sicily) and Prof. Mariano Licciardi (STEBICEF, UniPa), whose work was crucial to complete this research project. Collaboration had started with some previous projects, but their support and co-operation were essential to complete this project.

Further thanks go to Prof. Camarda as Co-Tutor who contributed to the realisation of this project and to my university education and to Prof. Olga Di Fede, the Tutor, for her support and expertise.